Journal of Catalysis 394 (2021) 131–141

Contents lists available at ScienceDirect

Journal of Catalysis

journal homepage: www.elsevier.com/locate/jcat

$Cr[CH(SiMe_3)_2]_3/SiO_2$ catalysts for ethene polymerization: The correlation at a molecular level between the chromium loading and the microstructure of the produced polymer

Giorgia A. Martino [a], Alessandro Piovano [a,*], Caterina Barzan [a], Yu-Kai Liao [a], Elena Morra [a], Kousou Hirokane [b], Mario Chiesa [a], Takashi Monoi [b], Elena Groppo [a]

[a] Department of Chemistry, NIS Centre and INSTM, University of Torino, via Giuria 7, 10125 Turin, Italy
[b] R&D Division, Japan Polychem Corporation, 1-1 Marunouchi 1-chome, Chiyoda-ku, Tokyo 100-8251, Japan

ARTICLE INFO

Article history:
Received 27 July 2020
Revised 16 November 2020
Accepted 21 December 2020
Available online 29 December 2020

Keywords:
Ethene polymerization
$Cr[CH(SiMe_3)_2]_3/SiO_2$ catalysts
Tandem catalysis
EPR spectroscopy
DR UV–vis spectroscopy
IR spectroscopy

ABSTRACT

Several spectroscopic techniques have been applied in a concerted way to investigate the local structure and the function of the chromium sites in a series of $Cr[CH(SiMe_3)_2]_3/SiO_2$ catalysts for ethene polymerization that differ in chromium loading and to correlate them with the microstructure of the produced polyethylene (PE). According to previous studies, the density of the produced PE is proportional to the Cr loading: the higher the Cr loading, the lower the PE density, because of an increase in the content of short-chain branching. Here, the nature of the branches and their enchainment in the polymer have been further investigated to determine the different properties of the produced polymers, and the differences detected have been traced back by spectroscopic analysis to the presence of two different types of Cr sites working in tandem: monografted $\equiv SiO—Cr[CH(SiMe_3)_2]_2$ species that are responsible for ethene oligomerization, and bis-grafted $(\equiv SiO—)_2CrCH(SiMe_3)_2$ species that account for ethene homo- and co-polymerization. The relative abundance of the two species depends on the chromium loading. Moreover, we have also found that carbon monoxide selectively poisons the sites responsible for ethene oligomerization, indicating a possible strategy for the fine regulation of the properties of the produced PE.

1. Introduction

Polyolefins are among the materials that marked the last century. Their success relies on both economic and environmental reasons (low cost, broad availability of the monomers, non-toxicity, easiness to recycle), as well as on their excellent physical and chemical properties, among which are chemical resistance (they are corroded only by strong oxidizing acids, such as nitric or sulfuric), high impact strength, and the broad temperature range of use (from −40 to almost + 100 °C) [1,2]. In particular, polyethylene (PE) is the most widely used polyolefin and, despite its very simple $(-CH_2-)_n$ composition, it is commercialized in hundreds of specialized grades, differing in the amount and the length of branching, the density, and the molecular weight distribution [3,4].

The new frontiers in olefin polymerization research forced an interpenetration between chemistry and engineering, aimed at matching the reaction mechanisms at a molecular scale with the reactor design [5,6]. From the chemical point of view, the research in this field has mostly been focused on the development of more efficient and tunable catalytic processes. Among these, chromium-based catalysts account for more than 60% of the world HDPE production [1], under the leadership of the Phillips catalyst and its modified variants [7]. This catalyst consists of chromium oxide species grafted onto a porous support material (typically amorphous silica), with a chromium concentration around 1 wt% or even lower (depending on the process). After calcination at a temperature higher than 600 °C, the oxidized precursor has to be reduced and alkylated to be active in ethene polymerization, either by ethene itself at 80–110 °C (during a certain induction time that precedes the polymerization reaction) or by some preactivating agents that shorten or even eliminate the induction time [7,8]. Alternative Cr catalysts are based on organochromium compounds. An early example is chromocene, which was at the basis of a commercial catalyst developed at Union Carbide [9–16], and later became an emblematic case study for active divalent chromium compounds. Other examples are open-ring bis-pentadienyl chromocene [17–20], $Cr(allyl)_2$ and $Cr(allyl)_3$ [13,21–26], β-stabilized Cr-alkyls [18,27–37], and $Cr(acetylacetonate)_3$ [38]. Most of these organochromium compounds have minimal or no activity for

* Corresponding author.
E-mail address: alessandro.piovano@unito.it (A. Piovano).

https://doi.org/10.1016/j.jcat.2020.12.022
0021-9517/

ethene polymerization until they are grafted onto a calcined oxide support material. This may be due to the fact that most of these complexes exist in solution as fully saturated dimers or even bigger oligomers, whereas they are stable as monomers only after anchoring onto a support [18]. Another possible effect of the support is associated with its electron-withdrawing character, which might induce a stronger positive charge on the chromium sites, promoting interaction with ethene [39].

Among ethene polymerization catalysts based on organochromium compounds, the $Cr[CH(SiMe_3)_2]_3/SiO_2$ ones stand out for high effectivity even at room temperature and without any preactivation treatment or scavengers, equaling the Phillips catalyst in both the polymerization activity and the grade of the produced polymer [29,30]. This observation fostered the hypothesis that alkylated Cr(III) sites might also be the active sites in the Phillips catalyst [40–44]. However, it has been also reported that the catalyst activity and, even more importantly, the microstructure of the PE produced strongly depend on both the chromium loading and the temperature at which silica was precalcined [30]. In particular, when the latter parameter is kept constant, an increase in the chromium loading causes a decrease in the activity per chromium site and a decrease in the polymer density. This effect is more drastic for the catalysts supported on silica activated at high temperature. For example, for catalysts on SiO_2 preactivated at 600 °C, it was found that a slight increase of the chromium content from 0.1 to 0.4 wt% caused a decrease of the polymer density from 0.9590 to 0.9065 g/cm^3, which was ascribed to the formation of short-chain branching (SCB) within the polymer (as observed by ^{13}C NMR) [29–31].

Altogether, these results suggested that two types of chromium sites coexist in these catalysts, co-working in tandem as already demonstrated for other systems [45–50]: those active in ethene oligomerization (hereafter Cr_{oligom}), which provide α-olefins, and those active in ethene homo- and copolymerization (hereafter Cr_{polym}), which polymerize ethene and incorporate the α-olefins produced at the former sites. The relative amounts of the two types of sites are a function of the chromium loading, with the Cr_{oligom}/Cr_{polym} ratio increasing with increasing chromium content. Some hypotheses on the molecular structure of the two types of sites were formulated in early works [30], which, however, were not supported by any experimental evidence. Here, we tackle this gap by investigating a series of $Cr[CH(SiMe_3)_2]_3/SiO_2$ catalysts, all prepared on silica precalcined at 600 °C, but differing in the chromium loading (from 0.2 to 0.5 wt%). The performance of these catalysts has been further evaluated at the extremes of the series, by running ethene polymerization in an autoclave and analyzing the properties of the products. Several spectroscopic techniques have been applied in situ to characterize the two types of chromium species at a molecular level and to understand the reaction conditions leading to one over the other.

2. Experimental

2.1. Catalyst synthesis

The $Cr[CH(SiMe_3)_2]_3$ precursor was synthesized from $(Me_3Si)_2$-CHCl and $CrCl_3$ as dark green crystals, following the procedure reported in Ref. [51]. The silica support (Sylopol952 from Grace, surface area 300 m^2/g and pore volume 1.6 cm^3/g) was calcined for 24 h at 600 °C under a stream of dry N_2. To obtain the $Cr[CH(SiMe_3)_2]_3/SiO_2$ catalysts, the same procedure described in Ref. [30] was adopted. Briefly, a hexane solution of $Cr[CH(SiMe_3)_2]_3$ was reacted for 1 h at 40 °C with the preactivated silica and then outgassed under vacuum at the same temperature until no volatiles appeared. Four different catalysts were synthetized with Cr loadings of 0.2, 0.3, 0.4, and 0.5 wt%, resulting in $n Cr[CH(SiMe_3)_2]_3/SiO_2$, where n denotes the Cr loading in wt.%.

2.2. Ethene polymerization tests

Ethene polymerization tests were carried out at 100 °C in a 2-L autoclave (P_{C2H4} = 14 bar, polymerization time = 60 min), using 800 mL of isobutane as solvent and without adding any co-catalyst or scavenger. The polymeric fractions of the products were analyzed by gel permeation chromatography (GPC) and ^1H and ^{13}C NMR spectroscopy, whereas the oligomeric fraction was scrutinized by means of gas chromatography (GC).

2.3. Characterization methods

2.3.1. Techniques

FT-IR spectra were collected in transmission mode by a Bruker Vertex70 instrument equipped with an MCT detector at a resolution of 2 cm^{-1}. Each sample was prepared in the form of a thin pellet (surface density ca. 50 mg/cm^2) directly inside a N_2-filled glove-box, inserted into a gold envelope, and placed in a quartz cell equipped with two KBr windows, which allowed sample manipulation without exposing it to air. The quartz cell was then interfaced with the spectrophotometer and further connected to a vacuum line that made it possible to send gaseous molecules onto the sample, monitoring the IR spectra at the same time.

UV–vis–NIR spectra were collected in diffuse reflectance mode (DR), using a Varian Cary5000 spectrophotometer, equipped with a reflectance sphere. Each sample was placed in powder form inside a bulb-shaped quartz cell terminating with a window in optical quartz (Suprasil). The cell was filled in the glove-box and successively interfaced with the spectrophotometer without exposing the sample to air.

EPR spectra were collected at the X-band (microwave frequency 9.76 GHz) with a Bruker ELEXYS 580 EPR spectrophotometer equipped with a super-high-Q cavity. Also in this case each sample, in powder form, was placed in the EPR tube inside the glove box. The measurements were performed at 77 K, placing the cell in a Dewar filled with liquid nitrogen. The magnetic field was measured with a Bruker ER035 M NMR gaussmeter. Data analysis was performed using the Easyspin software [52].

GC analysis of ethene oligomers was carried out on FID detector using a Shimadzu GCMS-QP2010 Ultra equipped with a DB-5MS column. The injection amount was 1 μL; the measurement conditions were from 40 to 325 °C, at a ramp-up rate of 10 °C/min.

GPC measurements of PE were carried out using a Waters 150C model equipped with a Shodex-AT806MS column, using 1,2-dichlorobenzene as eluent at 140 °C. The GPC curve was calibrated with standard polystyrene.

^{13}C NMR and ^1H NMR measurements were carried out on a Bruker AVANCE III 400 spectrometer. 1,2-Dichlorobenzene/bromobenzene-d5/hexamethyldisiloxane (mixing ratio: 80/20/1) was used as the solvent at 120 °C. The sample concentration was 0.1 g/2.4 mL and the pulse repetition time was 20 s in ^{13}C NMR and 2 s in ^1H NMR.

Polymer density measurements were performed according to JIS K-7112.

2.3.2. Methods

All catalysts were measured as originally produced and after interaction with ethene (the monomer) and CO (probe molecule), according to the following protocols.

1. Ethene was admitted directly into the measurement cell (ca. 100 mbar) at room temperature. The polymerization started immediately. The evolution of the IR and DR UV–vis spectra during the reaction was monitored continuously as a function of time,

while a single EPR spectrum was collected after 10 min of polymerization.

2. CO was dosed at room temperature, at equilibrium pressure P_{CO} = 50 mbar. An IR spectrum was collected under this condition (θ_{max}). Then the CO pressure was gradually lowered, until complete outgassing, and an IR spectrum was collected at each step.

3. Results and discussion

3.1. The $Cr[CH(SiMe_3)_2]_3$ precursor

Investigation of the $nCr[CH(SiMe_3)_2]_3/SiO_2$ catalysts cannot be exempted from the analysis of the $Cr[CH(SiMe_3)_2]_3$ precursor itself. The UV–vis and X-band CW-EPR spectra of the complex in hexane are reported in Fig. 1 and compared with those of a *hexa*-aquo Cr (III) complex.

The transmission UV–vis spectrum (spectrum 1 in Fig. 1a) is very similar to that reported in the literature for the analogous tris(bistrimethylsilylamido) Cr(III) trigonal complex, which has been interpreted on account of its D_{3h} geometry [53–56]. In more detail, the spectrum is characterized by two very intense bands at about 31000 and 25000 cm^{-1} having a ligand-to-metal charge-transfer nature, and by two weak and broad bands in the *d–d* region at about 14000 and 11000 cm^{-1}, assigned to $^4A'_2 \rightarrow (^4A''_1, ^4A''_2)$ and $^4A'_2 \rightarrow {}^4E$ *d–d* transitions, respectively [53,55]. The spectrum differs greatly from that characteristic of Cr(III) ions in an octahedral field (spectrum 2 in Fig. 1a), which shows two distinct *d–d* bands at ca. 22000 and 16000 cm^{-1} (attributed to $^4A_2 \rightarrow {}^4T_1$ and $^4A_2 \rightarrow {}^4T_2$ transitions, respectively) [57–65], and the intense charge-transfer bands shifted to much higher energy.

The corresponding EPR spectra reflect the differences observed in the UV–vis spectra. The EPR spectrum of $Cr[CH(SiMe_3)_2]_3$ (spectrum 1 in Fig. 1b) is characterized by a pseudo-axial pattern with effective *g* values $g_\perp \approx 4.0$. and $g_{II} \approx 2.0$, the latter component being rather weak. Using a *g*-value of 1.98, analysis indicates that the effective *g*-values of 4.0 and 2.0 require *D* to be greater than 23 GHz and *E* to be approximately zero [56,66–68]. The axial symmetry of the ZFS tensor is consistent with the D_{3h} symmetry of the molecule. The spectrum of the $CrCl_3$ aqueous solution (spectrum 2 in Fig. 1b), on the other hand, shows a totally different pattern, characterized by a broad feature at an effective $g \approx 2.0$ and a smaller feature at $g \approx 4.0$, well documented in the literature and due to Cr(III) in nearly octahedral coordination, either in a *hexa*-aquo complex or in a clustered form, where the intensity of the $g \approx 4.0$ feature is correlated to the degree of symmetry distortion [69].

The $Cr[CH(SiMe_3)_2]_3$ precursor was demonstrated to be active for ethene polymerization even without silica support, but only in the presence of an excess of MAO co-catalyst and in any case two order of magnitude less active than the corresponding silica-supported catalyst [70]. Hence, our investigation has focused on the $nCr[CH(SiMe_3)_2]_3/SiO_2$ catalysts, as follows.

3.2. Activity of the $nCr[CH(SiMe_3)_2]_3/SiO_2$ catalysts for ethene polymerization

The $nCr[CH(SiMe_3)_2]_3/SiO_2$ catalysts are active for ethene polymerization even without any co-catalyst and under conditions comparable to industrial ones [29], with the properties of the produced polymer depending on both the silica pretreatment and the Cr loading. In previous work, for catalysts supported on silica calcined at 600 °C, the chromium loading was varied in the range 0.1–0.4 wt% [30]. Here, we expanded this range in order to maximize the influence of the Cr loading on the catalyst performance, in terms of both ethene polymerization activity and PE properties. Table 1 reports the main results of the polymerization tests on the $0.1Cr[CH(SiMe_3)_2]_3/SiO_2$ and $0.5Cr[CH(SiMe_3)_2]_3/SiO_2$ catalysts.

The new test of ethene polymerization on the $0.1Cr[CH(SiMe_3)_2]_3/SiO_2$ catalyst well reproduces the data already reported in our previous work [30], while the $0.5Cr[CH(SiMe_3)_2]_3/SiO_2$ catalyst displays unprecedented performance, taking the postulated trend to an extreme as a function of the Cr loading. Briefly, for the $0.1Cr[CH(SiMe_3)_2]_3/SiO_2$ catalyst, the activity is very high and the produced polyethene is close to the HDPE obtained with a standard Phillips catalyst [7], whereas for the $0.5Cr[CH(SiMe_3)_2]_3/SiO_2$ catalyst the polymerization (whose yield per Cr site is much lower) is paired with the formation of oligomers, whose enchainment in the PE is responsible for the remarkably lower density of the polymer.

Whereas the differences in the produced polymers depending on Cr loading are a peculiarity of the $nCr[CH(SiMe_3)_2]_3/SiO_2$ catalytic systems and deserve further investigation, the drop in activity per Cr site at increasing Cr loading is a common problem for silica-supported catalysts for olefin polymerization, starting from the Phillips catalyst itself [7,71], and extending also to more advanced metallocene catalysts grafted on a support material [72–75]. Although the identification of the inactive species is still an open question (they appear the same as the active ones to most

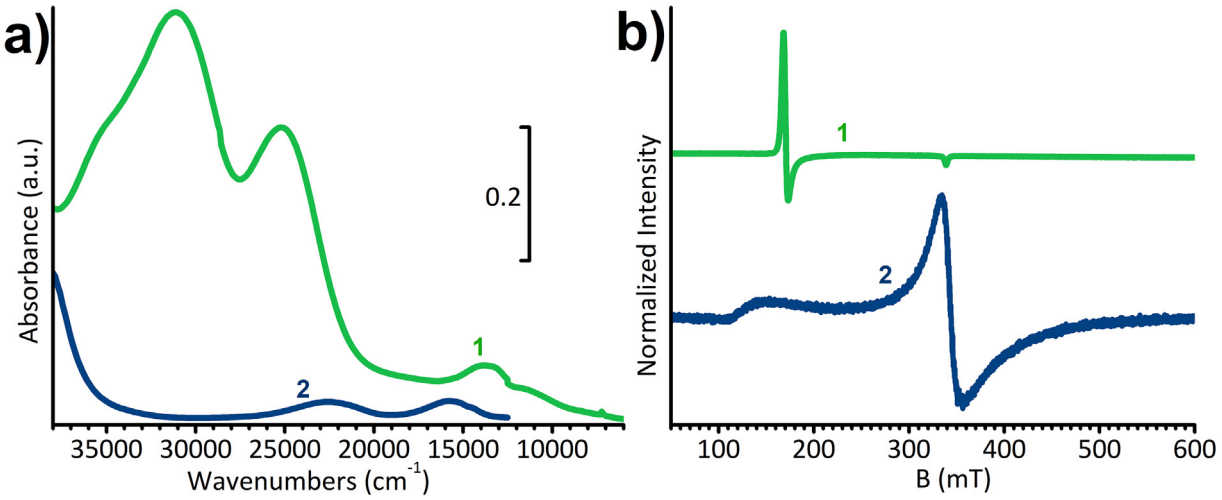

Fig. 1. Transmission UV–vis (a) and X-band CW-EPR (b) spectra of $Cr[CH(SiMe_3)_2]_3$ in hexane (1) and $CrCl_3$ in H_2O (2). The concentration of both solutions is on the order of 10^{-3} M.

Table 1
Results of ethene polymerization (P_{C2H4} = 14 bar) on nCr[CH(SiMe$_3$)$_2$]$_3$/SiO$_2$ catalysts in an autoclave at 100 °C.

Cr (wt.%)	Catalyst (mg)	Polymer yield (g)	Oligomer yield (g)	Activity (g_{PE}/mmol$_{Cr}$/h)	Polymer density (g/mL)
0.1	227.5	205 incorporated olefins: propene: 0 1-butene: <0.16 1-hexene: 0.49	none	51117	0.9555
0.5	198.2	12 incorporated olefins: propene: 0.25 1-butene: 0.19 1-hexene: 0.14	8	1049	0.8838

Note: The amounts of incorporated olefins with the polymer yield have been estimated from the PE analysis reported in Table S1.

of the characterization techniques), some possible reasons have been proposed in the past: the fact that at higher Cr content, more silica surface sites are occupied that are not suitable for catalysis [7], or the fact that the increasing proximity of the Cr species is detrimental for their activity [76].

Therefore, we have deepened the analysis of the products to clarify the PE microstructures and the nature of the oligomers and to correlate them with the different Cr species present on the catalysts at varying Cr loadings. Fig. 2a shows the GPC traces of the two polymers obtained with the 0.1Cr[CH(SiMe$_3$)$_2$]$_3$/SiO$_2$ and 0.5Cr[CH(SiMe$_3$)$_2$]$_3$/SiO$_2$ catalysts.

The two PE are characterized by comparable M_w (233000 and 232000 g/mol, respectively), although that produced with the 0.5Cr[CH(SiMe$_3$)$_2$]$_3$/SiO$_2$ catalyst has a molecular weight distribution broader than that obtained with the 0.1Cr[CH(SiMe$_3$)$_2$]$_3$/SiO$_2$ catalyst (19 instead of 15), with a pronounced shoulder at low M_w. Beside the slight differences in the chain length, the two polymers differ mostly in architecture (as reported in detail in Table S1 in the Supporting Information). In particular, the PE produced with the 0.5Cr[CH(SiMe$_3$)$_2$]$_3$/SiO$_2$ catalyst has a much higher content of both short-chain branches and saturated terminals (indicative of longer branches), while the slightly larger number of vinyl terminals per 1000C is compatible with the lower M_w resulting from the GPC plots in Fig. 2a. This structural difference reasonably accounts for the different density reported in Table 1 and can be explained by the different activity of the two catalysts in ethene oligomerization, although it is worth noting that the oligomer yield listed in Table 1 takes into account only the products at the end of the reaction, so the oligomers enchained in the polymers are not included.

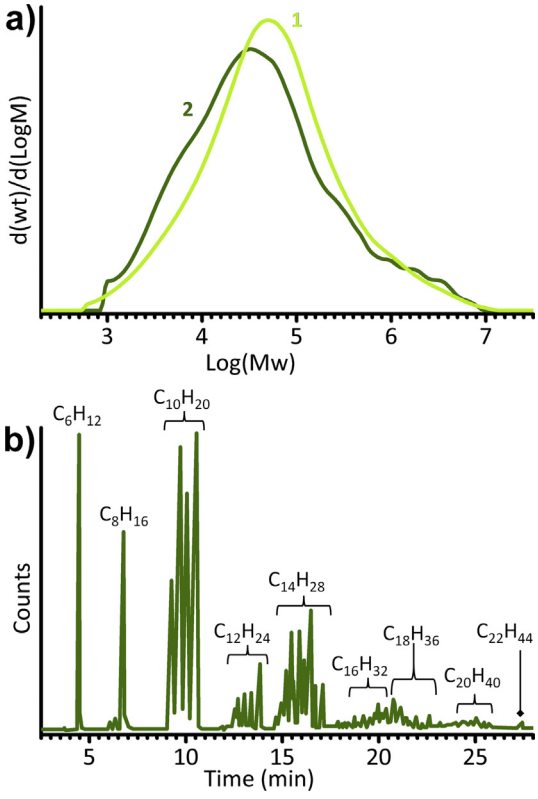

Fig. 2. (a) GPC plots of PE produced by 0.1Cr[CH(SiMe$_3$)$_2$]$_3$/SiO$_2$ (curve 1) and 0.5Cr[CH(SiMe$_3$)$_2$]$_3$/SiO$_2$ (curve 2) catalysts. (b) GC trace of the oligomeric olefins (C_nH_{2n}) produced by the 0.5Cr[CH(SiMe$_3$)$_2$]$_3$/SiO$_2$ catalyst.

The nature of the oligomers produced by the 0.5Cr[CH(SiMe$_3$)$_2$]$_3$/SiO$_2$ catalyst was investigated by GC analysis. The GC trace (reported in Fig. 2b) is constituted by several peaks, ascribed to a wide variety of even-number olefins ranging from C_6H_{12} (at an elution time of 4.5 min) to $C_{22}H_{44}$ (at 27 min); the only odd-number olefin produced is propene (responsible for methyl branches in Table S1), which has been proposed in the literature to derive from a side rearrangement and metathesis of the five-member Cr-metallacycle necessary for ethene oligomerization [77]. While shorter olefins are likely enchained in the growing polymers too fast to accumulate in the autoclave, the most abundant species in Fig. 2b are $C_{10}H_{20}$ (around 10 min), $C_{12}H_{24}$ (around 13 min), and $C_{14}H_{28}$ (around 16 min). Most of the long olefins stay as oligomers, but a minor fraction of them may also be incorporated into the polymer chains, thus accounting for the larger number of saturated terminals in the PE produced by the 0.5Cr[CH(SiMe$_3$)$_2$]$_3$/SiO$_2$ catalyst than in the PE produced by the 0.1Cr[CH(SiMe$_3$)$_2$]$_3$/SiO$_2$ catalyst (Table S1), and hence its much lower density. Increased branch length is typically associated with an improvement in the polymer mechanical properties (e.g., the impact strength and the ductility) [78,79]; therefore, understanding how to control PE branching by tuning the composition of the catalyst is of fundamental interest.

3.3. Identification of the two types of chromium sites in the nCr[CH(SiMe$_3$)$_2$]$_3$/SiO$_2$ catalysts

The nCr[CH(SiMe$_3$)$_2$]$_3$/SiO$_2$ catalysts display a bright green color, whose intensity increases with the chromium content. The corresponding DR UV–vis–NIR spectra are shown in Fig. 3a. They are characterized by a multitude of absorption bands, whose absolute intensity roughly scales with the chromium loading. The main bands are located at ca. 31000, 25000–22000 (very broad), 16000, and 11000 cm^{-1}. The bands at ca. 31000, 25000, and 11000 cm^{-1} are very similar to those observed in the spectrum of the Cr[CH(SiMe$_3$)$_2$]$_3$ precursor, while those at ca. 22000 and 16000 cm^{-1} resemble those characterizing the spectrum of $Cr(H_2O)_6^{3+}$. Hence, DR UV–vis–NIR spectroscopy gives a first confirmation of the

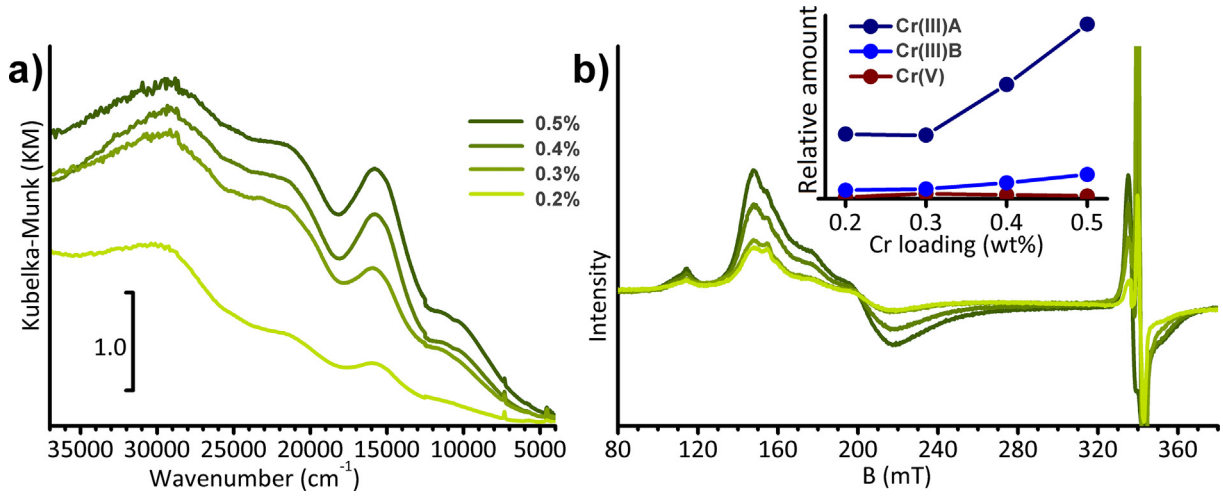

Fig. 3. DR UV–vis–NIR (a) and X-band CW-EPR (b) spectra of the *n*Cr[CH(SiMe$_3$)$_2$]$_3$/SiO$_2$ catalysts. The inset in (b) shows the relative amounts of Cr species as a function of Cr loading, obtained by multiplying the simulated percentages reported in Table S2 by the absolute intensity of the EPR spectra; Cr(V) includes both C and C' species of Table S2, Cr(III)B both B and B' species.

existence of two types of chromium sites, as suggested by early works [29,30]. On deeper observation, one may also notice that the relative intensity of the four bands is not constant with increasing chromium loading, with the band at 16000 cm^{-1} apparently more pronounced at higher Cr loadings with respect to the other bands. However, quantitative information cannot be extracted safely, due to the fact that the Lambert–Beer law is not valid for spectra collected in reflectance mode.

The EPR spectra of the four catalysts are shown in Fig. 3b. The spectra show significant differences with respect to the molecular precursor at both low field ($g \approx 4.0$) and central field ($g \approx 2.0$). At low field, the characteristic transition of Cr(III) species shows a complex spectral shape, which is indicative of an orthorhombic distortion of the Cr(III) species upon grafting on the surface. Simulation analysis (Fig. S1 and Table S2) provides evidence for the contribution of different species, which can be grouped into three main groups: a Cr(V) and two types of Cr(III). Note that these species remain the same in all the *n*Cr[CH(SiMe$_3$)$_2$]$_3$/SiO$_2$ catalysts, albeit in different amounts, indicating that the grafting reaction does not change significantly in the concentration interval. The two types of Cr(III) species (Cr(III)A and Cr(III)B) are characterized by different *D* and *E*/*D* values, where the latter parameter is a measure of the degree of local distortion. The relative abundance of these species was deduced by computer simulation (Fig. S1 and Table S2) and is reported in the inset of Fig. 3b for the four catalysts. The Cr(III) species characterized by the largest *E*/*D* value, Cr(III)A, accounts for approximately 70% of the spectral intensity, with an increasing trend as a function of the Cr loading. On the other hand, the relative abundance of the Cr(III)B species, characterized by lower *D* and *E*/*D* values, is found to be nearly constant in the same Cr loading interval and accounts for approximately 30% of the total EPR spectrum. The nature of the Cr(III)A and Cr(III)B species can be interpreted by analogy with the UV–vis spectroscopy. Cr(III)A, which is characterized by large *D* and *E*/*D* values, is amenable to the Cr[CH(SiMe$_3$)$_2$]$_3$ precursor, whereby the emergence of a rhombic tensor (*E*/*D* = 1/9) in Cr(III)B indicates a local distortion of the surface-bound complex. This latter species appears to be correlated to the UV–vis bands at 16,000 and 22,000 cm^{-1}, and is consistent with surface-coordinated species with distorted octahedral symmetry.

Finally, all the spectra show a small contribution at a magnetic field corresponding to $g \approx 2.0$, with a sharp signal at $g \approx 1.98$. This signal can be simulated assuming a $S = 1/2$ species with a slightly rhombic **g**. The spin Hamiltonian parameters are characteristic of Cr(V) species, often observed in supported Cr catalysts because of adventitious contamination, but negligible for the catalysis [80]. This signal will not be commented upon further.

Taken together, the DR UV–vis–NIR and EPR data can be interpreted in terms of at least two types of Cr(III) sites, as postulated by Monoi et al. on the basis of catalytic performance [30], whose relative amount depends on the chromium loading: (1) isolated low-coordinated Cr(III) sites, having a lower symmetry than that of the Cr[CH(SiMe$_3$)$_2$]$_3$ precursor, which are structurally the same in the four catalysts and whose amount increases with the chromium loading; (2) Cr(III) sites in a pseudo-octahedral field, likely connected to weak siloxane ligands and/or residual CH(SiMe$_3$)$_2$ groups anchored to the silica surface, whose amount is nearly constant with the chromium loading.

Organometallic compounds usually bind to the silica support by reaction with one or more surface hydroxyl groups, losing one or more organic ligands by hydrolysis and/or by opening the strained siloxane bridges [81–87], the latter path being favored for highly dehydroxylated silicas [88]. Scheme 1 reports three possible mechanisms for Cr[CH(SiMe$_3$)$_2$]$_3$ grafting on silica surface. Following path (a), Cr[CH(SiMe$_3$)$_2$]$_3$ reacts with two vicinal silanols, releasing two CH$_2$(SiMe$_3$)$_2$ groups and giving a bis-grafted chromium species, (≡SiO—)$_2$CrCH(SiMe$_3$)$_2$, likely stabilized by further interaction with the silica surface (e.g., through interaction with the siloxane bridges). Path (b) involves the reaction of Cr[CH(SiMe$_3$)$_2$]$_3$ with an isolated silanol and gives a monografted chromium species, ≡SiO—Cr[CH(SiMe$_3$)$_2$]$_2$, which is structurally similar to the Cr[CH(SiMe$_3$)$_2$]$_3$ precursor. The same monografted chromium species can be formed following path (c), which involves the opening of a siloxane bridge and the simultaneous formation of a ≡SiO—CH(SiMe$_3$)$_2$ species nearby. The occurrence of the first two paths is supported by IR spectroscopy. Indeed, by comparing the IR spectra of the four catalysts with that of bare silica (Fig. S2), it is evident that both isolated and vicinal silanols are partially consumed upon Cr[CH(SiMe$_3$)$_2$]$_3$ grafting. In particular, along with the series at increasing Cr loading, the ν(OH) band associated with vicinal silanols (at about 3540 cm^{-1}) is consumed more considerably than that ascribed to the isolated silanols (sharp band at 3745 cm^{-1}).

At this stage, we can reasonably hypothesize that the monografted ≡SiO—Cr[CH(SiMe$_3$)$_2$]$_2$ species are those showing spectroscopic properties more similar to those of the Cr[CH(SiMe$_3$)$_2$]$_3$ precursor (i.e., bands at ca. 31000, 25000, and 11000 cm^{-1} in the

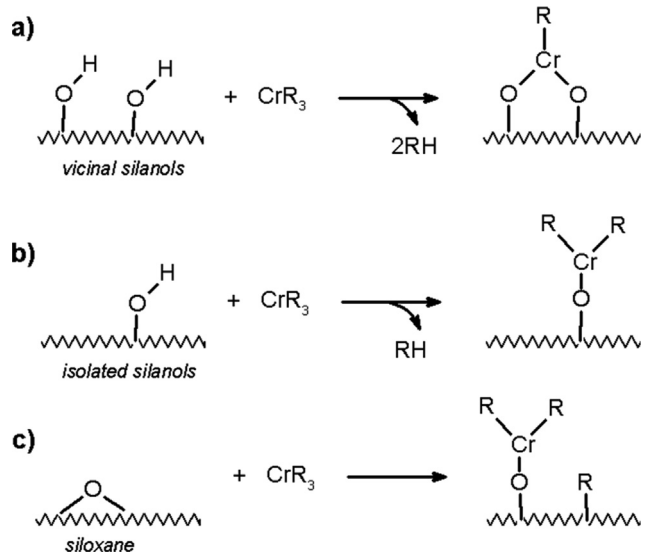

Scheme 1. Schematic representation of the possible routes for $Cr[CH(SiMe_3)_2]_3$ grafting on silica surface by reaction with different surface functional groups. R stands for the $CH(SiMe_3)_2$ group, which is a quite encumbering ligand. The schemes are simplified for clarity and do not take into account the possible presence of siloxane ligands in the chromium coordination sphere.

DR UV–vis–NIR spectra, and Cr(III)A in EPR analysis). The bis-grafted $(\equiv SiO—)_2CrCH(SiMe_3)_2$ species, instead, are those showing spectroscopic manifestations close to those of a chromium complex in a distorted octahedral field (i.e., bands at ca. 22000 and 16000 cm^{-1} in the DR UV–vis–NIR spectra, and Cr(III)B in EPR analysis). Remembering that the seminal works on the $nCr[CH(SiMe_3)_2]_3/SiO_2$ catalysts correlated the increase of the Cr loading with an increase in the number of SCB within the produced polymer [29,30], we can roughly associate the monografted $\equiv SiO—Cr[CH(SiMe_3)_2]_2$ sites to the reaction of ethene oligomerization to α-olefins (Cr_{oligom}) and the bis-grafted $(\equiv SiO—)_2CrCH(SiMe_3)_2$ sites to the reactions of ethene polymerization and copolymerization with the α-olefins (Cr_{polym}). As a matter of fact, both DR UV–vis–NIR and EPR spectroscopies point out that the amount of the former increases with respect to the amount of the latter upon increasing the chromium loading. This statement will be further discussed and confirmed in the following section.

3.4. Reactivity of the chromium sites toward ethene

The activity of the investigated catalysts toward ethene under mild conditions was investigated by means of in situ IR, DR UV–vis–NIR, and EPR spectroscopy. Fig. 4 shows the time-resolved IR spectra collected during reaction of ethene at room temperature on the $0.2Cr[CH(SiMe_3)_2]_3/SiO_2$ and $0.5Cr[CH(SiMe_3)_2]_3/SiO_2$ catalysts, which represent the two extremes of our catalyst series. As soon as ethene is admitted into the reaction cell, polymerization occurs readily, as testified by the fast growth of several absorption bands in both $\nu(CH_x)$ and $\delta(CH_x)$ regions. In particular, four absorption bands are observed in the $\nu(CH_x)$ region, typical of a branched PE: the two bands at 2925 and 2855 cm^{-1} are assigned to the asymmetric and symmetric stretching of the CH_2 moieties in the chains, while the two bands at 2960 and 2875 cm^{-1} are assigned to the asymmetric and symmetric stretching of the CH_3 terminations [89–92]. The corresponding bending modes are respectively responsible for the bands at 1463 and 1378 cm^{-1} (as magnified in the right insets), whose relative intensities give a rough estimation of the number of terminations with respect to the length of the chains (relatively higher for ethene polymerization on the $0.5Cr[CH(SiMe_3)_2]_3/SiO_2$ catalyst in Fig. 4a than for ethene polymerization on the $0.2Cr[CH(SiMe_3)_2]_3/SiO_2$ catalyst in Fig. 4b). The growing alkyl chains (i.e., both the polymer backbones and the long branches) interact rapidly with the SiOH groups at the silica surface, as indicated by the downward shift of the band at 3750 cm^{-1} to 3695 cm^{-1} during the polymerization.

Simultaneously, two absorption bands are observed at 3075 and 1641 cm^{-1} (magnified in the left and middle insets), which are assigned to $\nu(=CH_2)$ and $\nu(C=C)$, respectively, and are much more evident for the $0.5Cr[CH(SiMe_3)_2]_3/SiO_2$ catalyst (Fig. 4a) than for the $0.2Cr[CH(SiMe_3)_2]_3/SiO_2$ one (Fig. 4b). The simultaneous observation of CH_3 groups and of unsaturated CH_x species indicate the production of α-olefins and their enchainment in the growing PE. Both processes seem to be favored at higher chromium loading, in good agreement with the polymer properties reported in the literature [30]. It is interesting to observe that, under our experimental conditions, the rate of α-olefin production is much higher than the rate of their enchainment in the growing PE. Indeed, in both experiments, a very broad band at 3550 cm^{-1} grows during the reaction, at the expense of that at 3750 cm^{-1}, providing evidence for interaction of the isolated silanols at the silica surface with the C=C moieties, including the vinyl terminals and the α-olefins [48].

Fig. 5 shows the DR UV–vis–NIR and EPR spectra of the $0.2Cr[CH(SiMe_3)_2]_3/SiO_2$ catalyst and those during and/or after reaction with ethene (the results on the other catalysts are reported in Fig. S3). As soon as ethene is admitted into the reaction cell, the DR UV–vis–NIR spectra (Fig. 5a) rapidly decrease in intensity in the whole spectral region. This indicates the formation of a large amount of PE, which modifies the scattering properties of the catalyst powder [93]. Indeed, the presence of the polymer is testified by the appearance of new absorption bands in the NIR region (inset in Fig. 5a), which are assigned to the overtones and combination modes of the $\nu(CH_x)$ and $\delta(CH_x)$ vibrational modes of the polymer chains. The very first spectrum collected in the presence of ethene clearly shows that the bands more affected by PE formation are those at 22000 and 16000 cm^{-1} (ascribed to the bis-grafted $(\equiv SiO—)_2CrCH(SiMe_3)_2$ species), while that at 11000 cm^{-1} (assigned to the monografted $\equiv SiO—Cr[CH(SiMe_3)_2]_2$ species) initially does not change. This observation indicates that the bis-grafted $(\equiv SiO—)_2CrCH(SiMe_3)_2$ species are those initially masked by the polymer or, in other words, are those mostly responsible for ethene polymerization, as anticipated in the previous section.

Analysis of the EPR spectra in Fig. 5b under the same reaction conditions indicates a spectral change in the $g \approx 4$ region upon the polymerization reaction, demonstrating that the Cr(III) species undergo a change in the local environment. Such a change is logically expected for the monografted $\equiv SiO—Cr[CH(SiMe_3)_2]_2$ species, hypothesizing a metallacycle mechanism for ethene oligomerization [7,40,47,94–97]. On the other hand, if we consider a Cossee–Arlman polymerization mechanism on the bis-grafted $(\equiv SiO—)_2CrCH(SiMe_3)_2$ species [98], we can assume a distortion in the local structure of the $(\equiv SiO—)_2Cr[polymer]$ propagating sites induced by the growth of the polymer chains.

All in all, the DR UV–vis–NIR and EPR spectra provide definite evidence that ethene oligomerization occurs at the monografted $\equiv SiO—Cr[CH(SiMe_3)_2]_2$ sites (Cr_{oligom}), while homo- and copolymerization are due to the bis-grafted $(\equiv SiO—)_2CrCH(SiMe_3)_2$ ones (Cr_{polym}). Very recently, similar catalytic behavior has been demonstrated for chromium *tris*(amide) complexes supported on oxides and activated by several Al-alkyl co-catalysts [99], but this is the first time that the cooperation between the two Cr species has been fully characterized, from their origins and the control of their relative abundance to their working under reaction conditions, and finally to post-synthesis modifications discussed hereafter.

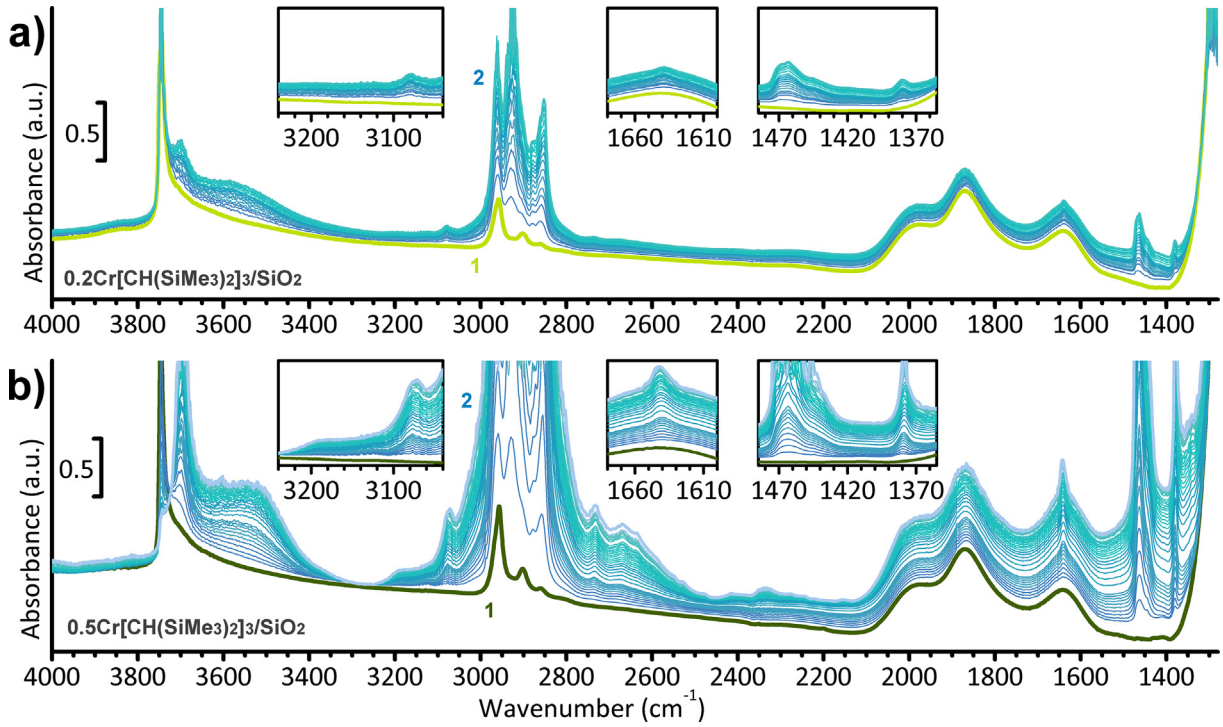

Fig. 4. Time-resolved IR spectra collected during ethene polymerization at room temperature (P_{C2H4} = 100 mbar) on 0.2Cr[CH(SiMe$_3$)$_2$]$_3$/SiO$_2$ (part a) and 0.5Cr[CH(SiMe$_3$)$_2$]$_3$/SiO$_2$ (part b). In both cases, spectrum 1 was collected before ethene interaction, while spectrum 2 was collected after about 20 min of reaction. All the intermediate spectra were collected every 5 s. The insets report magnifications in the ν(=CH$_x$), ν(C = C), and δ(CH$_x$) regions (left, middle, and right, respectively).

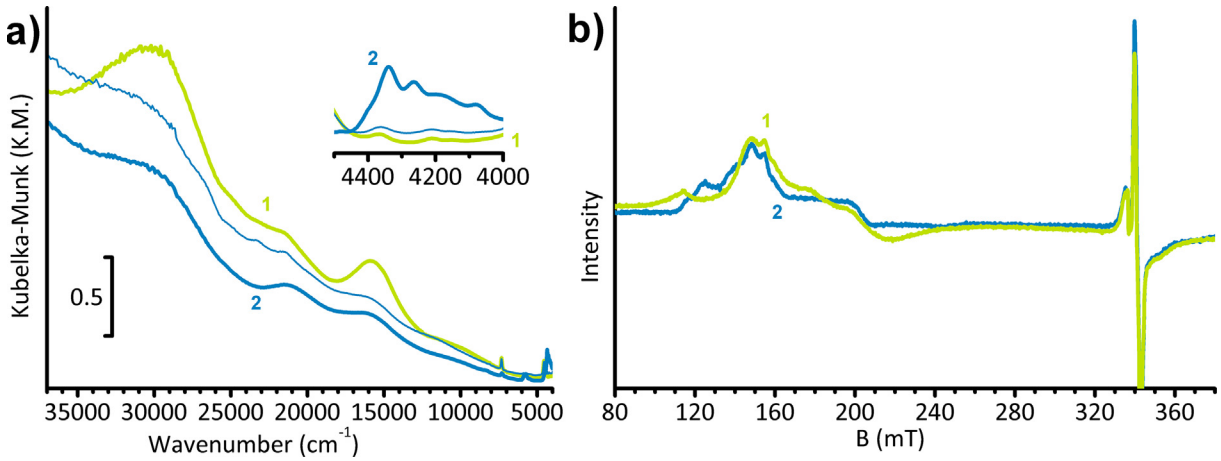

Fig. 5. Evolution of the DR UV–vis–NIR (a) and X-band CW EPR (b) spectra during ethene polymerization at room temperature (P_{C2H4} = 100 mbar) on the 0.2Cr[CH(SiMe$_3$)$_2$]$_3$/SiO$_2$ catalyst. In both cases, spectrum 1 was collected before ethene interaction, while spectrum 2 was collected after about 10 min of reaction. The intermediate DR UV–vis–NIR spectrum was collected after 3 min. The inset in (a) shows the NIR region, containing the overtones and combination modes of the ν(CH$_x$) and δ(CH$_x$) vibrational modes of the polymer chains.

3.5. Reactivity of the chromium sites toward CO

Additional details on the Cr sites discussed so far have been achieved by monitoring with IR spectroscopy the CO adsorption on the four catalysts. As a matter of fact, not only CO is a well-established molecular probe for the surface properties of catalytic materials in general [100], but in the specific case of supported Cr species it has also been proved to be able to discriminate between mono- and bis-grafted sites [47,96].

Fig. 6 shows the IR spectra of CO adsorbed at room temperature at the maximum CO coverage (θ_{max}) on the four catalysts, after subtraction of the spectra of the catalysts prior to CO dosage. For all the samples, the spectra are dominated by two intense absorption bands in the region 2160–1860 cm^{-1} (Fig. 5a). Moreover, weaker bands are observed in the region 1700–1500 cm^{-1} (Fig. 5b), and at ca. 3400 cm^{-1} (very broad), while weak negative bands are observed in the region ν(CH$_x$), which indicate that a small fraction of the alkyl groups are perturbed by the interaction with CO. Going into more details, the following comments can be made.

1. Starting from the most intense bands, the region 2160–1860 cm^{-1} is that characteristic of ν(C≡O) for classical metal carbonyls [8]. The first band, quite broad, is located at 2039 cm^{-1} (with a shoulder at 2050 cm^{-1}), and the second, extremely narrow,

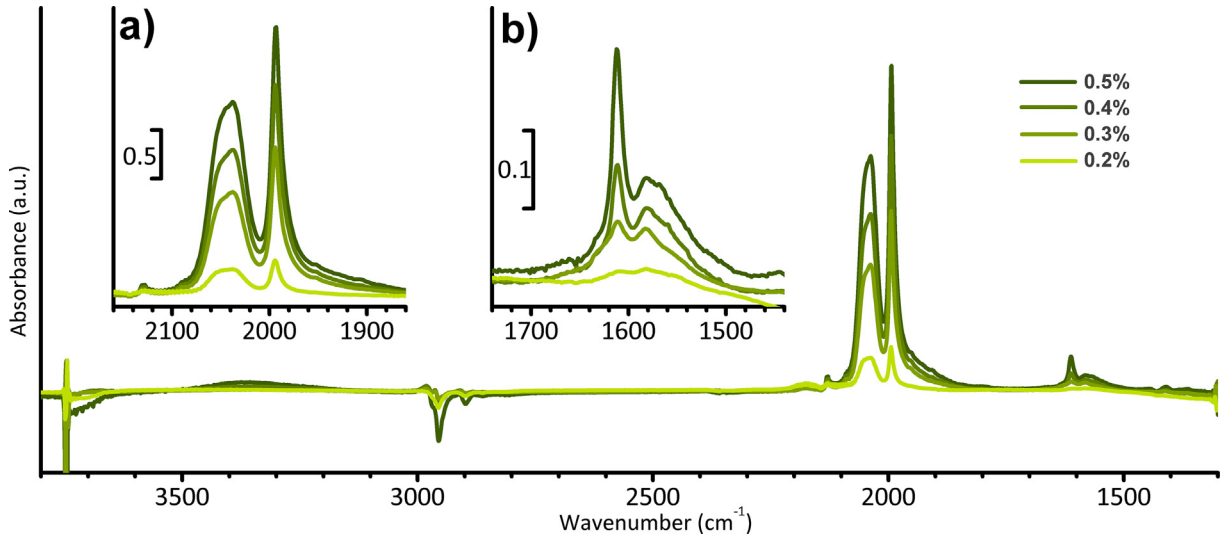

Fig. 6. IR spectra of CO adsorbed at room temperature on the *n*Cr[CH(SiMe$_3$)$_2$]$_3$/SiO$_2$ catalysts (P_{CO} = 50 mbar) after subtraction of the spectra of the catalysts prior to CO dosage. (a) and b) show magnifications of the spectra in the regions ν(C≡O) and ν(C═O), respectively.

at 1993 cm^{-1}. A similar two-band profile is characteristic of highly symmetric tricarbonyl metal complexes [57,101]. For example, the spectrum of (η^6-C$_6$H$_6$)Cr(CO)$_3$ shows two bands at 1966 and 1898 cm^{-1} [102–105]. The two bands are assigned to the non-degenerate total symmetric stretching and to the doubly degenerate total asymmetric stretching of the M(CO)$_3$ moiety. Hence, these spectra indicate that chromium tricarbonyls are formed when our catalysts are contacted with CO.

2. As far as the weak bands in the region 1700–1500 cm^{-1} are concerned (Fig. 5b), they are assigned to the ν(C═O) vibration of chromium acyl species, originating from the insertion of CO into the Cr–C bond [106–110]. Indeed, it is known that CO has the capability to insert into metal–carbon bonds, and in olefin polymerization catalysis this is a strategy often adopted to quench the polymerization activity in case of reactor fouling [111].

3. In both spectral intervals, the intensity of the absorption bands roughly scales with the chromium loading; hence in principle all the Cr sites might be involved in the reaction with CO. However, we can attempt a deeper assignment. Indeed, we have demonstrated previously that CO is an excellent probe to discriminate between mono- and bis-grafted chromium species; that is, the corresponding carbonyls have completely different spectroscopic properties [8]. Moreover, the bis-grafted Cr$_{polym}$ sites are already sixfold coordinated, so that insertion of three additional ligands looks unlikely. Hence, we ascribe the bands at 2039 and 1993 cm^{-1} to chromium tricarbonyls formed on the monografted Cr$_{oligom}$ sites (≡SiO—Cr[CH(SiMe$_3$)$_2$]$_2$(CO)$_3$), while we assume that the bis-grafted Cr$_{polym}$ sites do not coordinate CO in a molecular form. In contrast, we expect that the bis-grafted species are involved in the formation of chromium acyls, although we cannot exclude a contribution of the monografted ones also. In this respect, it is worth noticing that we have recently observed a similar phenomenon on the bis-grafted Cr(IV) bis-alkyl species formed upon reaction of the Cr(VI)/SiO$_2$ Phillips catalyst with triethylaluminum (TEAl) [97].

4. Finally, the very broad band at ca. 3400 cm^{-1} is attributed to the presence of some OH groups in H-bonding interaction. We interpret this observation as due to the interaction of the ≡SiO—Cr[CH(SiMe$_3$)$_2$]$_2$(CO)$_3$ tricarbonyls with the OH groups at the silica surface, justified by the large dimensions of these complexes.

The chromium tricarbonyls and chromium acyl species formed in the presence of CO are only partially reversible upon CO removal. The IR spectra collected during the controlled decrease of the CO pressure (Fig. S4) are quite complex and suggest the transformation of most of the chromium tricarbonyls into chromium monocarbonyls, which are irreversible even after prolonged outgassing at room temperature (path a in Scheme S1). Moreover, the absorption bands ascribed to both ν(OH) and ν(CH$_x$) decrease slightly in intensity after CO removal. A tentative explanation is that the ≡SiO—Cr[CH(SiMe$_3$)$_2$]$_2$(CO)$_3$ tricarbonyls in interaction with the silanols via H-bonding are not stable when CO is removed, but react rapidly as ≡SiO—Cr[CH(SiMe$_3$)$_2$]$_2$ + ≡Si-OH →(≡SiO—)$_2$-Cr[CH(SiMe$_3$)$_2$] + CH$_2$(SiMe$_3$)$_2$. The CH$_2$(SiMe$_3$)$_2$ compound thus formed can be outgassed together with the CO molecules by decreasing the gas pressure (path b in Scheme S1). According to this hypothesis, a small fraction of the monografted Cr$_{oligom}$ species are irreversibly transformed into bis-grafted Cr$_{polym}$ species after the interaction with CO. This phenomenon is more probable at high chromium loading, where the probability of finding a monografted Cr$_{oligom}$ site in proximity to a OH group is greater. Confirmation for this mechanism comes from the observation that, upon dosing with CO a second time, the intensity of the ν(C≡O) bands is lower (i.e., a few Cr$_{oligom}$ sites were lost and no longer available for CO adsorption), whereas from the second cycle onward no substantial further changes are observed (Fig. S5).

The data discussed so far indicate that CO is not an innocent probe for the chromium sites, at least for the Cr$_{oligom}$ ones. To understand whether or not the Cr$_{polym}$ sites are also irreversibly modified by CO, we followed the activity of the nCr[CH(SiMe$_3$)$_2$]$_3$/SiO$_2$ catalysts in ethene polymerization after exposure to CO by IR spectroscopy. The results for the 0.5Cr[CH(SiMe$_3$)$_2$]$_3$/SiO$_2$ catalyst are shown in Fig. 7. The spectroscopic manifestations of the oligomers (ν(=CH$_2$) at 3075 cm^{-1} and ν(C═C) at 1641 cm^{-1}, left and middle insets) are almost absent, while those of PE are well visible. This behavior clearly indicates that CO selectively poisons most of the Cr$_{oligom}$ (as discussed above), while the majority of the Cr$_{polym}$ sites are unaffected, either because they are completely inaccessible to CO or because the eventually formed acyl species do not prevent ethene from coordinating to Cr and inserting into the Cr–R bond, thus growing the alkyl chain. Furthermore, in looking at the δ(CH$_x$) region, it is also worth noticing that the band of δ(CH$_3$) at 1378 cm^{-1} is almost invisible (the number of terminations is negligible with respect to the length of the chains) and that the band of δ(CH$_2$) is split into two components at 1463 (as before) and 1472 cm^{-1}, the former related to the amorphous phase of PE and

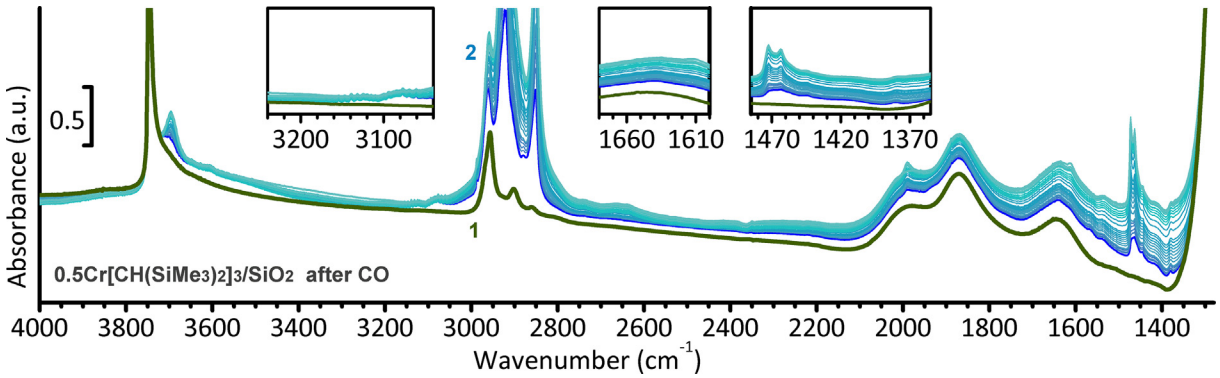

Fig. 7. Time-resolved IR spectra collected during ethene polymerization at room temperature (P_{C2H4} = 100 mbar) on the 0.5Cr[CH(SiMe$_3$)$_2$]$_3$/SiO$_2$ catalyst after interaction with CO. Spectrum 1 was collected before ethene interaction, while spectrum 2 was collected after about 20 min of reaction. All the intermediate spectra were collected every 5 s. The insets report magnifications in the ν(=CH$_x$), ν(C=C), and δ(CH$_3$) regions (left, middle and right, respectively).

the latter to the crystalline one [91], meaning that CO poisoning also affects the physical state of the produced polymer.

4. Conclusions

In this work we have conducted a systematic characterization of a series of Cr[CH(SiMe$_3$)$_2$]$_3$/SiO$_2$ catalysts for ethene polymerization, prepared by grafting the Cr[CH(SiMe$_3$)$_2$]$_3$ precursor onto a highly dehydroxylated silica and differing in chromium concentration. According to the early literature (and here verified by catalytic tests), the chromium loading has a drastic influence on the properties of the PE produced: a higher chromium loading leading to a PE with lower density. This behavior was ascribed to the co-presence of two types of Cr(III) sites, which either oligomerize ethene affording α-olefins or homo- and copolymerize it to give a branched PE. However, experimental evidence on the nature of the chromium sites at a molecular level was still missing.

By applying DR UV–vis–NIR, X-band CW EPR, and IR spectroscopies we have been able to discriminate the two types of Cr(III) sites in the Cr[CH(SiMe$_3$)$_2$]$_3$/SiO$_2$ catalysts, at the same time determining their local structure, their relative concentrations, and their function. Monografted ≡SiO—Cr[CH(SiMe$_3$)$_2$]$_2$ species, having a low coordination and maintaining most of the structural properties of the Cr[CH(SiMe$_3$)$_2$]$_3$ precursor, are responsible for ethene oligomerization (Cr$_{oligom}$ in Scheme 2a) up to $C_{22}H_{44}$ compounds (as determined by GC analysis). Bis-grafted (≡SiO—)$_2$CrCH(SiMe$_3$)$_2$ species, highly coordinated in an almost octahedral geometry, are responsible for ethene polymerization (Cr$_{polym}$ in Scheme 2b).

Overall, the spectroscopic techniques revealed a trend in the relative proportions between the Cr$_{polym}$ and the Cr$_{oligom}$ sites, the latter being relatively more abundant at higher Cr content, in good agreement with what was suggested by the analysis of the produced polymers. This trend can be explained by considering that the bis-grafted Cr$_{polym}$ species can be formed only if there are two vicinal OH species at the silica surface (Scheme 1a), a condition progressively less probable with increasing amounts of Cr species on the surface. As a matter of fact, the OH population depends on the type of silica and on its calcination temperature [112,113], which are the same for all the catalysts: a silica activated at 600 °C has a residual density of surface OH of ca. 1.5 OH per nm^2, which corresponds to 37–38 OH groups per Cr species for the 0.1Cr[CH(SiMe$_3$)$_2$]$_3$/SiO$_2$ catalyst and 7–8 OH groups per Cr species for the 0.5Cr[CH(SiMe$_3$)$_2$]$_3$/SiO$_2$ one. Among these OH groups, only a limited fraction are constituted by vicinal OH groups available for forming Cr$_{polym}$ sites, which are evidently more consumed at higher chromium loadings. Hence, as the chromium concentration increases, the formation of monografted Cr$_{oligom}$ species is favored, by reaction either with isolated silanols or with siloxane bridges (Schemes 1b and 1c, respectively).

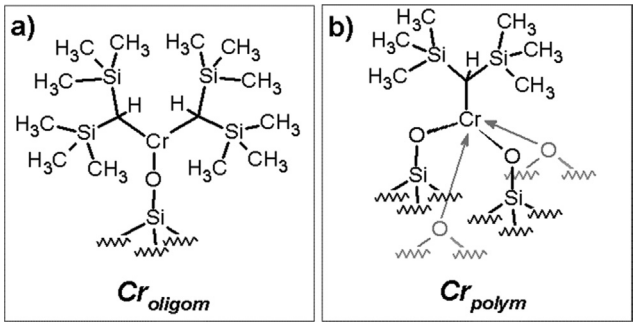

Scheme 2. Local structure of the mono- and bis-grafted chromium species on the *n*Cr[CH(SiMe$_3$)$_2$]$_3$/SiO$_2$ catalysts, as determined by spectroscopic methods. The two species are associated with ethene oligomerization and homo- and copolymerization, respectively.

CO was found to be a non-innocent probe for the chromium sites, forming chromium carbonyls on the Cr$_{oligom}$ sites, and partially inserting into the Cr–C bond to form chromium acyls, likely on both Cr$_{oligom}$ and Cr$_{polym}$ sites. However, it irreversibly poisons only the Cr$_{oligom}$ sites, and hence its use turns out to be an effective way to tune the catalytic activity of the Cr[CH(SiMe$_3$)$_2$]$_3$/SiO$_2$ catalysts.

Overall, the synergetic use of three spectroscopic techniques allowed deciphering at a molecular scale the local structures of the two types of chromium species present in the Cr[CH(SiMe$_3$)$_2$]$_3$/SiO$_2$ catalysts, their relative amounts, and their interconnections. These results are particularly relevant from the perspective of rationally developing innovative catalysts for ethene conversion to polymers with widely adjustable properties. On a more general ground, this work represents a paradigmatic example of the complexity of a silica-supported catalyst, even when prepared by grafting a well-defined organometallic precursor. Indeed, we demonstrated that two types of chromium sites are originated starting from the same chromium precursor, which are characterized by very different molecular structure, different electronic properties, and completely diverse function, and we disclosed their sensitivity to chemical treatments.

Declaration of Competing Interest

The authors declare that they have no known competing financial interests or personal relationships that could have appeared to influence the work reported in this paper.

Acknowledgments

This paper is part of a project that has received funding from the European Union's Horizon 2020 research and innovation program under Marie Skłodowska-Curie Grant Agreement 813209.

References

[1] J. Jansz, Global PO&E News Analysis (2015).
[2] Ellen MacArthur Foundation, The New Plastics Economy: Rethinking the Future of Plastics, McKinsey & Company, 2016.
[3] A.J. Peacock, Handbook of Polyethylene. Structures, properties and applications. , New York Basel 2000.
[4] T.E. Nowlin, Business and Technology of the Global Polyethylene Industry, Wiley-Scrivener, New York, 2014.
[5] D. Stoiljković, R. Radičević, M. Janković, Dependence of the structural parameters and properties of low density polyethylene on the synthesis conditions, J. Serb. Chem. Soc. 64 (1999) 577–587.
[6] E. Tioni, J.P. Broyer, V. Monteil, T. McKenna, Influence of reaction conditions on catalyst behavior during the early stages of gas phase ethylene homo- and copolymerization, Ind. Eng. Chem. Res. 51 (2012) 14673–14684.
[7] M.P. McDaniel, A Review of the Phillips Supported Chromium Catalyst and Its Commercial Use for Ethylene Polymerization, Adv. Catal. 53 (2010) 123–606.
[8] E. Groppo, G.A. Martino, A. Piovano, C. Barzan, The active sites in the Phillips catalysts: origins of a lively debate and a vision for the future, ACS Catal. 8 (2018) 10846–10863.
[9] M.P. McDaniel, J.N. Short, Catalyst comprising a phosphate and with a bis-(cyclopentadienyl)chromium(II) compound, U.S. Patent 4,424,139, 1984.
[10] M.P. McDaniel, J.N. Short, Polymerization process using a catalyst comprising a phosphate and with a bis-(cyclopentadienyl)chromium(II) compound, U.S. Patent 4,690,990, 1987.
[11] M.P. McDaniel, J.N. Short, Ethylene polymer produced using a catalyst comprising a phosphate and with a bis-(cyclopentadienyl)chromium(II) compound, US Patent 4803253, 1989.
[12] F.J. Karol, G.L. Brown, J.M. Davison, Chromocene-based catalysts for ethylene polymerization: Kinetic parameters, J. Polym. Sci. A 11 (1973) 413–424.
[13] F.J. Karol, R.N. Johnson, Ethylene polymerization studies with supported cyclopentadienyl, arene, and allyl chromium catalysts, J. Polym. Sci. Polym. Chem. Ed. 13 (1975) 1607–1617.
[14] F.J. Karol, Studies with High Activity Catalysts for Olefin Polymerization, Catal. Rev. 26 (1984) 557–595.
[15] B. Rebenstorf, T. Lindblad, Amorphous AlPO4 as catalyst support.1. FTIR study of co adsorbed on chromocene and trimethylsilylchromocene reacted with AlPO4, Acta Chem. Scand. 44 (1990) 789–792.
[16] B. Rebenstorf, The Phillips catalyst (Cr(VI) silica-gel) modified by $(NH_4)_2SiF_6$ - Its influence on the chromium surface species, J. Mol. Catal. 66 (1991) 59–71.
[17] T.D. Newbound, J.W. Freeman, D.R. Wilson, M.S. Kralik, A.T. Patton, C.F. Campana, R.D. Ernst, Structural and reaction chemistry of the open chromocene bis(2,4-dimethylpentadienyl)chromium, Organometallics 6 (1987) 2432–2437.
[18] P.D. Smith, M.P. McDaniel, Ethylene polymerization catalysts from supported organotransition metal complexes: I. Pentadienyl derivatives of Ti, V, and Cr, J. Polym. Sci. A Polym. Chem. 27 (1989) 2695–2710.
[19] M.P. McDaniel, Controlling polymer properties with the Phillips chromium catalysts, Ind. Eng. Chem. Res. 27 (1988) 1559–1564.
[20] J.W. Freeman, D.R. Wilson, R.D. Ernst, P.D. Smith, D.D. Klendworth, M.P. McDaniel, Ethylene polymerization over organochromium catalysts: A comparison between closed and open pentadienyl ligands, J. Polym. Sci. A Polym. Chem. 25 (1987) 2063–2075.
[21] O.M. Bade, R. Blom, M. Ystenes, Chromium allyls on silica: A study of structure and reactivity, Organometallics 17 (1998) 2524–2533.
[22] D.G.H. Ballard, Pi and Sigma Transition Metal Carbon Compounds as Catalysts for the Polymerization of Vinyl Monomers and Olefins, Adv. Catal. (1973) 263–325.
[23] D.G.H. Ballard, E. Jones, A.J.P. Pioli, P.A. Robinson, R.J. Wyatt, Polymerisation process, U.S. Patent 3,840,508, 1974.
[24] D.G.H. Ballard, A.W. Parkins, P.A. Robinson, S.D. Ibekwe, M.F. Lappert, R. Pearce, Organo-metallic compounds, U.S. Patent 3,969,386, 1976.
[25] Y. Yermakov, V. Zakharov, One-Component Catalysts for Polymerization of Olefins, Adv. Catal. 24 (1975) 173–219.
[26] Y.I. Yermakov, Supported Catalysts Obtained by Interaction of Organometallic Compounds of Transition Elements with Oxide Supports, Catal. Rev. 13 (1976) 77–120.
[27] M.P. McDaniel, P.D. Smith, in Olefin polymerization using supported pentadienyl derivative-transition metal complexes, US Patent 5075394, 1991.
[28] M.P. McDaniel, P.D. Smith, in Olefin polymerization using supported pentadienyl derivative-transition metal complexes, US Patent 5200379, 1993.
[29] H. Ikeda, T. Monoi, Y. Sasaki, Performance of the Cr[CH(SiMe3)2]3/SiO2 catalyst for ethylene polymerization compared with the performance of the phillips catalyst, J. Polym. Sci. A Polym. Chem. 41 (2003) 413–419.
[30] T. Monoi, H. Ikeda, Y. Sasaki, Y. Matsumoto, Ethylene Polymerization with Silica-Supported Cr[CH(SiMe3) 2]3 Catalyst. Effect of Silica Calcination Temperature and Cr Content, Polym. J. 35 (2003) 608–611.
[31] T. Monoi, Y. Sasaki, Silica-supported Cr[N(SiMe3)(2)](3)/isobutylalumoxane catalyst for selective ethylene trimerization, J. Mol. Catal. A Chem. 187 (2002) 135–141.
[32] J. Amor Nait Ajjou, G.L. Rice, S.L. Scott, Kinetics and mechanisms of thermally induced alkane eliminations from silica-supported bis(alkyl)chromium(IV) and -vanadium(IV) complexes, J. Am. Chem. Soc. 120 (1998) 13436–13443.
[33] J. Amor Nait Ajjou, S.L. Scott, Reactions of tetraalkylchromium(IV) with silica: Mechanism of grafting and characterization of surface organometallic complexes, Organometallics 16 (1997) 86–92.
[34] J. Amor Nait Ajjou, S.L Scott, A kinetic study of ethylene and 1-hexene homo- and copolymerization catalyzed by a silica-supported Cr(IV) complex: Evidence for propagation by a migratory insertion mechanism, J. Am. Chem. Soc. 122 (2000) 8968–8976.
[35] J. Amor Nait Ajjou, S.L. Scott, V. Paquet, Synthesis and characterization of silica-stabilized chromium(IV) alkylidene complexes, J. Am. Chem. Soc. 120 (1998) 415–416.
[36] S.L. Scott, J. Amor Nait Ajjou, Surface organometallic investigation of the mechanism of ethylene polymerization by silica-supported Cr catalysts, Chem. Eng. Sci. 56 (2001) 4155–4168.
[37] S.L. Scott, A. Fu, L.A. MacAdams, Effect of silica type and grafting method on the reactivity of tetraneopentylchromium(IV) towards and on silica, Inorg. Chim. Acta 361 (2008) 3315–3321.
[38] G. Henrici-Olivé, S. Olivé, Vanadium and Chromium Catalysts for Polymerization of Ethylene, Angew. Chem. 10 (1971) 776–786.
[39] G.A. Martino, C. Barzan, A. Piovano, A. Budnyk, E. Groppo, Tracking the reasons for the peculiarity of Cr/Al2O3 catalyst in ethylene polymerization, J. Catal. 357 (2018) 206–212.
[40] M.F. Delley, F. Núñez-Zarur, M.P. Conley, A. Comas-Vives, G. Siddiqi, S. Norsic, V. Monteil, O.V. Safonova, C. Copéret, Proton transfers are key elementary steps in ethylene polymerization on isolated chromium(III) silicates, Proc. Natl. Acad. Sci. U.S.A. 111 (2014) 11624–11629.
[41] M.P. Conley, M.F. Delley, F. Núñez-Zarur, A. Comas-Vives, C. Copéret, Heterolytic Activation of C-H Bonds on CrIII–O Surface Sites Is a Key Step in Catalytic Polymerization of Ethylene and Dehydrogenation of Propane, Inorg. Chem. 54 (2015) 5065–5078.
[42] C. Copéret, F. Allouche, K.W. Chan, M.P. Conley, M.F. Delley, A. Fedorov, I.B. Moroz, V. Mougel, M. Pucino, K. Searles, K. Yamamoto, P.A. Zhizhko, Bridging the Gap between Industrial and Well-Defined Supported Catalysts, Angew. Chem. Int. Ed. 57 (2018) 6398–6440.
[43] A. Fong, Y. Yuan, S.L. Ivry, S.L. Scott, B. Peters, Computational kinetic discrimination of ethylene polymerization mechanisms for the Phillips (Cr/SiO<inf>2</inf>) catalyst, ACS Catal. 5 (2015) 3360–3374.
[44] C. Brown, A. Lita, Y. Tao, N. Peek, M. Crosswhite, M. Mileham, J. Krzystek, R. Achey, R. Fu, J.K. Bindra, M. Polinski, Y. Wang, L.J. Van De Burgt, D. Jeffcoat, S. Profeta, A.E. Stiegman, S.L. Scott, Mechanism of Initiation in the Phillips Ethylene Polymerization Catalyst: Ethylene Activation by Cr(II) and the Structure of the Resulting Active Site, ACS Catal. 7 (2017) 7442–7455.
[45] J.-C. Wasilke, S.J. Obrey, R.T. Baker, G.C. Bazan, Concurrent Tandem Catalysis, Chem. Rev. 105 (2005) 1001–1020.
[46] M. Frediani, C. Fiel, W. Kaminsky, C. Bianchini, L. Rosi, Tandem copolymerization: An effective control of the level of branching and molecular weight distribution, Macromol. Symp. 236 (2006) 124–133.
[47] C. Barzan, D. Gianolio, E. Groppo, C. Lamberti, V. Monteil, E.A. Quadrelli, S. Bordiga, The effect of hydrosilanes on the active sites of the phillips catalyst: The secret for in situ olefin generation, Chem. Eur. J. 19 (2013) 17277–17282.
[48] C. Barzan, E. Groppo, E.A. Quadrelli, V. Monteil, S. Bordiga, Ethylene polymerization on a SiH_4-modified Phillips catalyst: detection of in situ produced a-olefins by operando FT-IR spectroscopy, Phys. Chem. Chem. Phys. 14 (2012) 2239–2245.
[49] D. Cicmil, J. Meeuwissen, A. Vantomme, J. Wang, I.K. van Ravenhorst, H.E. van der Bij, A. Munoz-Murillo, B.M. Weckhuysen, Polyethylene with Reverse Co-monomer Incorporation: From an Industrial Serendipitous Discovery to Fundamental Understanding, Angew. Chem. 54 (2015) 13073–13079.
[50] A. Piovano, K.S. Thushara, E. Morra, M. Chiesa, E. Groppo, Unraveling the Catalytic Synergy between Ti3+ and Al3+ Sites on a Chlorinated Al2O3: A Tandem Approach to Branched Polyethylene, Angew. Chem. Int. Ed. 55 (2016) 11203–11206.
[51] G.K. Barker, M.F. Lappert, J.A.K. Howard, Silylmethyl and Related Complexes. Part 6. l Preparation, Properties, and Crystal and Molecular Structure of Tris [bis(trimethylsilyl)methyl]- chromium(III); the Chemistry of Related Compounds of Titanium(III), Vanadium(III), Zirconium(IV), and Hafnium (IV), J. Chem. Soc. Dalton Trans. (1978) 734–740.
[52] S. Stoll, A. Schweiger, EasySpin, a comprehensive software package for spectral simulation and analysis in EPR, J. Magn. Reson. 178 (2006) 42–55.
[53] G.M. Sheldrick, W.S. Sheldrick, Crystal and molecular structure of tris[bis (trimethylsilyl)amino]aluminium, Al[N(SiMe3)2]3, J. Chem. Soc. A 2279–2282 (1969).
[54] E.C. Alyea, D.C. Bradley, R.G. Copperthwaite, Three-co-ordinated transition metal compounds. Part I. The preparation and characterization of tris (bistrimethylsilylamido)-derivatives of scandium, titanium, vanadium, chromium, and iron, J. Chem. Soc. Dalton Trans. (1972) 1580–1584.
[55] E.C. Alyea, D.C. Bradley, R.G. Copperthwaite, K.D. Sales, Three-co-ordinated transition-metal compounds. Part II. Electronic spectra and magnetism of tris (bistrimethylsilylamido)derivatives of scandium, titanium, vanadium, chromium, and iron, J. Chem. Soc. Dalton Trans. (1973) 185–191.

[56] P.G. Eller, D.C. Bradley, M.B. Hursthouse, D.W. Meek, Three coordination in metal complexes, Coord. Chem. Rev. 24 (1977) 1–95.
[57] B.N. Figgis, Introduction to ligand fields, Wiley, New York, 1966.
[58] A. Zecchina, E. Garrone, G. Ghiotti, C. Morterra, E. Borello, On the chemistry of Silica supported chromium ions. I. Characterization of the samples, J. Phys. Chem. 79 (1975) 966–972.
[59] B.M. Weckhuysen, L.M. Deridder, R.A. Schoonheydt, A quantitative diffuse reflectance spectroscopy study of supported chromium catalysts, J. Phys. Chem. 97 (1993) 4756–4763.
[60] B.M. Weckhuysen, I.E. Wachs, R.A. Shoonheydt, Surface chemistry and spectroscopy of chromium in inorganic oxides, Chem. Rev. 96 (1996) 3327–3349.
[61] B.M. Weckhuysen, B. Schoofs, R.A. Schoonheydt, Mobility of chromium in inorganic oxides - Spectroscopic fingerprinting of oxidation states and coordination environments, J. Chem. Soc. Faraday Trans. 93 (1997) 2117–2120.
[62] B.M. Weckhuysen, R.A. Schoonheydt, Recent progresses in diffuse reflectance spectroscopy of supported metal oxide catalysts, Catal. Today 49 (1999) 441–451.
[63] B.M. Weckhuysen, A.A. Verberckmoes, A.R. DeBaets, R.A. Schoonheydt, Diffuse reflectance spectroscopy of supported chromium oxide catalysts: A self-modeling mixture analysis, J. Catal. 166 (1997) 160–171.
[64] B.M. Weckhuysen, I.E. Wachs, R.A. Schoonheydt, Spectroscopic characterization of supported Cr and Cr, Ti catalysts: Interaction with probe molecules, Stud. Surf. Sci. Catal. 91 (1995) 151–158.
[65] M. Cieslak-Golonka, Spectroscopy of chromium(VI) species, Coord. Chem. Rev. 109 (1991) 223–249.
[66] D.C. Bradley, R.G. Copperthwaite, S.A. Cotton, K.D. Sales, J.F. Gibson, Three-co-ordinated transition-metal compounds. Part III. Electron spin resonance studies on tris(bistrimethylsilylamido)derivatives of titanium, chromium, and iron, J. Chem. Soc. Dalton Trans. (1973) 191–194.
[67] M.F. Delley, G. Lapadula, F. Núñez-Zarur, A. Comas-Vives, V. Kalendra, G. Jeschke, D. Baabe, M.D. Walter, A.J. Rossini, A. Lesage, L. Emsley, O. Maury, C. Copéret, Local Structures and Heterogeneity of Silica-Supported M(III) Sites Evidenced by EPR, IR, NMR, and Luminescence Spectroscopies, J. Am. Chem. Soc. 139 (2017) 8855–8867.
[68] E. Morra, G.A. Martino, A. Piovano, C. Barzan, E. Groppo, M. Chiesa, In Situ X- and Q-Band EPR Investigation of Ethylene Polymerization on Cr/SiO2 Phillips Catalyst, J. Phys. Chem. C 122 (2018) 21531–21536.
[69] D. Collison, F.E. Mabbs, A method for the simulation of powder electron spin resonance spectra when S > ½; application to the iron–molybdenum–sulphur protein of nitrogenase and of some [Fe4S4(SR)4]3– clusters, J. Chem. Soc. Dalton Trans. 1565–1574 (1982).
[70] H. Ikeda, T. Monoi, K. Ogata, H. Yasuda, Ethylene Polymerizations with Alkyl-, Disilylamino- and Cyclopentadienylchromium/MMAO Initiators, Macromol. Chem. Phys. 202 (2001) 1806–1811.
[71] J.P. Hogan, Chapter 6 - Catalysis of the Phillips Petroleum Company Polyethylene Process, in: Applied Industrial Catalysis, Academic Press, New York, 1983, pp. 149–176.
[72] M.P. McDaniel, E.A. Benham, S.J. Martin, K.S. Collins, J.L. Smith, G.R. Hawley, C. E. Wittner, M.D. Jensen, Compositions that can produce polymers, U.S. Patent 6300271, 2001.
[73] M.P. McDaniel, E.A. Benham, K.S. Collins, A.P. Eaton, M.D. Jensen, J.L. Martin, G.R. Hawley, Organometal catalyst compositions,U.S. Patent 6613852, 2003.
[74] M.R. Ribeiro, A. Deffieux, M.F. Portela, Supported Metallocene Complexes for Ethylene and Propylene Polymerizations: Preparation and Activity, Ind. Eng. Chem. Res. 36 (1997) 1224–1237.
[75] J.R. Severn, J.C. Chadwick, Immobilisation of homogeneous olefin polymerisation catalysts. Factors influencing activity and stability, J. Chem. Soc. Dalton Trans. 42 (2013) 8979–8987.
[76] E.M.E. van Kimmenade, A.E.T. Kuiper, Y. Tamminga, P.C. Thune, J.W. Niemantsverdriet, A surface science model for the Phillips ethylene polymerization catalyst: thermal activation and polymerization activity, J. Catal. 223 (2004) 134–141.
[77] B.P. Liu, H. Nakatani, M. Terano, Mechanistic implications of the unprecedented transformations of ethene into propene and butene over Phillips CrO_x/SiO_2 catalyst during induction period, J. Mol. Catal. A 201 (2003) 189–197.
[78] T.M. Liu, W.E. Baker, The effect of the length of the short chain branch on the impact properties of linear low density polyethylene, Polym. Eng. Sci. 32 (1992) 944–955.
[79] R. Gao, X. He, Y. Shao, Y. Hu, H. Zhang, Z. Liu, B. Liu, Effects of Branch Content and Branch Length on Polyethylene Crystallization: Molecular Dynamics Simulation, Macromol. Theory Simul. 25 (2016) 303–311.
[80] B.M. Weckhuysen, L.M. Deridder, P.J. Grobet, R.A. Schoonheydt, Redox behavior and dispersion of supported chromium catalysts, J. Physi. Chem. 99 (1995) 320–326.
[81] J.P. Candlin, H. Thomas, Supported Organometallic Catalysts, in: Homogeneous Catalysis—II, American Chemical Society, 1974, pp. 212-239.
[82] P. Mania, S. Conrad, R. Verel, C. Hammond, I. Hermans, Thermal restructuring of silica-grafted –CrO2Cl and –VOCl2 species, J. Chem. Soc. Dalton Trans. 42 (2013) 12725–12732.
[83] D. Gajan, C. Coperet, Silica-supported single-site catalysts: to be or not to be? A conjecture on silica surfaces, New J. Chem. 35 (2011) 2403–2408.
[84] R. Anwander, SOMC@PMS. Surface organometallic chemistry at periodic mesoporous silica, Chem. Mat. 13 (2001) 4419–4438.
[85] L. Lefort, M. Chabanas, O. Maury, D. Meunier, C. Copéret, J. Thivolle-Cazat, J.-M. Basset, Versatility of silica used as a ligand: effect of thermal treatments of silica on the nature of silica-supported alkyl tantalum species, J. Organomet. Chem. 593–594 (2000) 96–100.
[86] C. Barzan, A. Piovano, L. Braglia, G.A. Martino, C. Lamberti, S. Bordiga, E. Groppo, Ligands Make the Difference! Molecular Insights into CrVI/SiO2 Phillips Catalyst during Ethylene Polymerization, J. Am. Chem. Soc. 139 (2017) 17064–17073.
[87] M.H. Valkenberg, W.F. Hölderich, Preparation and use of hybrid organic–inorganic catalysts, Catal. Rev. 44 (2002) 321–374.
[88] C. Copéret, A. Comas-Vives, M.P. Conley, D.P. Estes, A. Fedorov, V. Mougel, H. Nagae, F. Núñez-Zarur, P.A. Zhizhko, Surface Organometallic and Coordination Chemistry toward Single-Site Heterogeneous Catalysts: Strategies, Methods, Structures, and Activities, Chem. Rev. 116 (2016) 323–421.
[89] S. Krimm, C.Y. Liang, G.B.B.M. Sutherland, Infrared Spectra of High Polymers. II. Polyethylene, J. Chem. Phys. 25 (1956) 549–562.
[90] J.R. Nielsen, A.H. Woollett, Vibrational Spectra of Polyethylenes and Related Substances, J. Chem. Phys. 26 (1957) 1391–1401.
[91] D. Chelazzi, M. Ceppatelli, M. Santoro, R. Bini, V. Schettino, High-pressure synthesis of crystalline polyethylene using optical catalysis, Nat. Mater. 3 (2004) 470–475.
[92] A. Piovano, E. Morra, M. Chiesa, E. Groppo, Tuning the Ti3+ and Al3+ Synergy in an Al2O3/TiClx Catalyst to Modulate the Grade of the Produced Polyethylene, ACS Catal. 7 (2017) 4915–4921.
[93] C. Barzan, A. Piovano, L. Braglia, G.A. Martino, C. Lamberti, S. Bordiga, E. Groppo, Ligands Make the Difference! Molecular Insights into CrVI/SiO2 Phillips Catalyst during Ethylene Polymerization, J. Am. Chem. Soc. 139 (2017) 17064–17073.
[94] A. Brückner, Monitoring transition metal ions (TMI) in oxide catalysts during (re)action: The power of operando EPR, Phys. Chem. Chem. Phys. 5 (2003) 4461–4472.
[95] A. Brückner, J.K. Jabor, A.E.C. McConnell, P.B. Webb, Monitoring structure and valence state of chromium sites during catalyst formation and ethylene oligomerization by in situ EPR spectroscopy, Organometallics 27 (2008) 3849–3856.
[96] G.A. Martino, A. Piovano, C. Barzan, S. Bordiga, E. Groppo, The Effect of Al-Alkyls on the Phillips Catalyst for Ethylene Polymerization: The Case of Diethylaluminum Ethoxide (DEALE), Top. Catal. 61 (2018) 1465–1473.
[97] G.A. Martino, A. Piovano, C. Barzan, J. Rabeah, G. Agostini, A. Brückner, G. Leone, G. Zanchin, T. Monoi, E. Groppo, Rationalizing the effect of triethylaluminum on the Cr/SiO2 Phillips catalysts, ACS Catal. 10 (2020) 2694–2706.
[98] P. Cossee, Ziegler-Natta catalysis I. Mechanism of polymerization of α-olefins with Ziegler-Natta catalysts, J. Catal. 3 (1964) 80–88.
[99] M.J. Lamb, D.C. Apperley, M.J. Watson, P.W. Dyer, The Role of Catalyst Support, Diluent and Co-Catalyst in Chromium-Mediated Heterogeneous Ethylene Trimerisation, Top. Catal. 61 (2018) 213–224.
[100] C. Lamberti, A. Zecchina, E. Groppo, S. Bordiga, Probing the surfaces of heterogeneous catalysts by in situ IR spectroscopy, Chem. Soc. Rev. 39 (2010) 4951–5001.
[101] G.L. Miessler, D.A. Tarr, Inorganic Chemistry, Pearson Education International, Northfield, Minnesota.
[102] T.E. Bitterwolf, K.A. Lott, A.J. Rest, J. Mascetti, Photolysis of Group VI metal carbonyls, (η6-C6H6)Cr(CO)3, (η5-C5H5)Mn(CO)3, (η5-CH3C5H4)Mn(CO)3 and (η5-C5H5)Re(CO)3 in Nujol at 77 K, J. Organomet. Chem. 419 (1991) 113–126.
[103] R. Cohen, E. Weitz, J.M.L. Martin, M.A. Ratner, Arene hapticity in (C6H6)Cr(CO)(n) (n=1-5) complexes: A DFT study of singlet and triplet energy surfaces, Organometallics 23 (2004) 2315–2325.
[104] M.A.H. Alamiry, N.M. Boyle, C.M. Brookes, M.W. George, C. Long, P. Portius, M. T. Pryce, K.L. Ronayne, X.-Z. Sun, M. Towrie, K.Q. Vuong, Unusually Slow Photodissociation of CO from (η6-C6H6)Cr(CO)3 (M = Cr or Mo): A Time-Resolved Infrared Matrix Isolation, and DFT Investigation, Organometallics 28 (2009) 1461–1468.
[105] S. Chavan, J.G. Vitillo, M.J. Uddin, F. Bonino, C. Lamberti, E. Groppo, K.P. Lillerud, S. Bordiga, Functionalization of UiO-66 metal-organic framework and highly cross-linked polystyrene with Cr(CO)3: In situ formation, stability, and photoreactivity, Chem. Mater. 22 (2010) 4602–4611.
[106] F. Calderazzo, Synthesis and properties of transition metal to carbon bonds, in: A.B.P. Lever (Ed.), Coordination Chemistry–XIV, Butterworth-Heinemann, 1973, pp. 453–474.
[107] F. Calderazzo, Synthetic and Mechanistic Aspects of Inorganic Insertion Reactions. Insertion of Carbon Monoxide, Angew. Chem. Int. Ed. Engl. 16 (1977) 299–311.
[108] F. Calderazzo, Synthesis and reactivity of carbon-bonded transition elements, Pure Appl. Chem. 50 (1978) 49.
[109] K.W. Barnett, D.L. Beach, S.P. Gaydos, T.G. Pollmann, Methyl and acetyl complexes of chromium and tungsten. Observations on metal—carbon bond strength variations in the chromium triad, J. Organomet. Chem. 69 (1974) 121–130.
[110] R.B. Hitam, R. Narayanaswamy, A.J. Rest, Matrix isolation studies of the bonding of acetyl groups in the co-ordinatively unsaturated species acetyltetracarbonylmanganese and acetylmonocarbonyl(η-cyclopentadienyl)iron, J. Chem. Soc. Dalton Trans. 615–618 (1983).
[111] A.D. Caunt, The determination of active centres in olefin polymerisation, Br. Polym. J. 13 (1981) 22–26.
[112] L.T. Zhuravlev, Surface characterization of amorphous silica - a review of work from the former USSR, Colloids Surf. A 74 (1993) 71–90.
[113] L.T. Zhuravlev, The surface chemistry of amorphous silica. Zhuravlev model, Colloids Surf. A 173 (2000) 1–38.